NeuroImage: Clinical 4 (2014) 711–717

Contents lists available at ScienceDirect

NeuroImage: Clinical

journal homepage: www.elsevier.com/locate/ynicl

In vivo axonal transport deficits in a mouse model of fronto-temporal dementia

Tabassum Majid [a,b], Yousuf O. Ali [c,d], Deepa V. Venkitaramani [e], Ming-Kuei Jang [e], Hui-Chen Lu [c,d,f,g], Robia G. Pautler [a,b,g,*]

[a] Interdepartmental Program in Translational Biology and Molecular Medicine, Baylor College of Medicine, Houston, TX, USA
[b] Department of Molecular Physiology and Biophysics, Baylor College of Medicine, USA
[c] Department of Pediatrics, Baylor College of Medicine, Houston, TX, USA
[d] The Cain Foundation Laboratories, Jan and Dan Duncan Neurological Research Institute at Texas Children's Hospital, Houston, TX, USA
[e] Institute for Applied Cancer Science, The University of Texas M.D. Anderson Cancer Center, Houston, TX, USA
[f] Developmental Biology Program, Baylor College of Medicine, Houston, TX, USA
[g] Department of Neuroscience, Baylor College of Medicine, Houston, TX, USA

ARTICLE INFO

Article history:
Received 12 October 2013
Received in revised form 12 February 2014
Accepted 14 February 2014
Available online 31 March 2014

Keywords:
MEMRI
MRI
Axonal transport
Tau
Alzheimer's disease
Fronto-temporal dementia

ABSTRACT

Background: Axonal transport is vital for neurons and deficits in this process have been previously reported in a few mouse models of Alzheimer's disease prior to the appearance of plaques and tangles. However, it remains to be determined whether axonal transport is defective prior to the onset of neurodegeneration. The rTg4510 mouse, a fronto-temporal dementia and parkinsonism-17 (FTDP-17) tauopathy model, over-express tau-P301L mutation found in familial forms of FTDP-17, in the forebrain driven by the calcium–calmodulin kinase II promoter. This mouse model exhibits tau pathology, neurodegeneration in the forebrain, and associated behavioral deficits beginning at 4–5 months of age.

Animal model: rTg4510 transgenic mice were used in these studies. Mice were given 2 μL of $MnCl_2$ in each nostril 1 h prior to Magnetic Resonance Imaging (MRI). Following $MnCl_2$ nasal lavage, mice were imaged using Manganese enhanced Magnetic Resonance Imaging (MEMRI) Protocol with TE = 8.5 ms, TR = 504 ms, FOV = 3.0 cm, matrix size = 128 × 128 × 128, number of cycles = 15 with each cycle taking approximately 2 min, 9 s, and 24 ms using Paravision software (BrukerBioSpin, Billerica, MA). During imaging, body temperature was maintained at 37.0 °C using an animal heating system (SA Instruments, Stony Brook, NY).

Data analysis: Resulting images were analyzed using Paravision software. Regions of interest (ROI) within the olfactory neuronal layer (ONL) and the water phantom consisting of one pixel (ONL) and 9 pixels (water) were selected and copied across each of the 15 cycles. Signal intensities (SI) of ONL and water phantom ROIs were measured. SI values obtained for ONL were then normalized the water phantom SI values. The correlation between normalized signal intensity in the ONL and time were assessed using Prism (GraphPad Software, San Diego, CA).

Results: Using the MEMRI technique on 1.5, 3, 5, and 10-month old rTg4510 mice and littermate controls, we found significant axonal transport deficits present in the rTg4510 mice beginning at 3 months of age in an age-dependent manner. Using linear regression analysis, we measured rates of axonal transport at 1.5, 3, 5, and 10 months of age in rTg4510 and WT mice. Axonal transport rates were observed in rTg4510 mice at 48% of WT levels at 3 months, 40% of WT levels at 5 months, and 30% of WT levels at 10 months of age. In order to determine the point at which tau appears in the cortex, we probed for phosphorylated tau levels, and found that pSer262 is present at 3 months of age, not earlier at 1.5 months of age, but observed no pathological tau species until 6 months of age, months after the onset of the transport deficits. In addition, we saw localization of tau in the ONL at 6 months of age.

Discussion: In our study, we identified the presence of age-dependent axonal transport deficits beginning at 3 months of age in rTg4510 mice. We correlated these deficits at 3 months to the presence of hyperphosphorylated tau in the brain and the presence within the olfactory epithelium. We observed tau pathology not only in the soma of these neurons but also within the axons and processes of these neurons. Our characterization of axonal transport in this tauopathy model provides a functional time point that can be used for future therapeutic interventions.

* Corresponding author at: One Baylor Plaza, MC:335, Houston, TX 77030, USA.

http://dx.doi.org/10.1016/j.nicl.2014.02.005

1. Introduction

Fronto-temporal dementia (FTD) is a neurodegenerative disorder that accounts for approximately 20% of all pre-senile dementia cases (Wszolek et al., 2006). It is characterized by changes in reasoning, movement, speech, and language and primarily affects the frontal and anterior temporal lobes in the brain (Ingram and Spillantini, 2002). Diagnosis of FTD is difficult due to the fact that patients can display a wide variation in the severity of symptoms. Over the past quarter century, a proportion of FTD cases have been discovered to have a strong familial component. One of these includes FTD with parkinsonism (FTDP-17) (Wszolek et al., 2006). This form of FTD is associated with tau tangle pathology due to mutations in the microtubule associated protein tau (MAPT) gene on chromosome 17 (Wszolek et al., 2006). Current therapies have focused on delaying disease progression, but have been limited in their success. Part of the challenge in this area is identifying an optimal time point for intervention.

Autopsies from FTDP-17 patients have revealed neurofibrillary tau tangle pathology in the frontal and temporal lobes of the brain (Wszolek et al., 2006); (Snowden et al., 2002); (Goedert et al., 2012). The tau mutations in FTDP-17 have been linked to two major pathological outcomes (Combs and Gamblin, 2012). The first of these is disruption in alternative splicing that leads to a higher ratio of 4R tau rather than 3R tau. The second being the disruption of tau binding to microtubules in neurons, causing the accelerated accumulation of aggregate forms of tau as well as an increase in the formation of tau filaments (Wszolek et al., 2006). One of the more predominant mutations in the tau gene that is associated with FTDP-17 is the P301L mutation (Bird et al., 1999). This mutation results in a phenotype where the average age of onset is between 41 and 50 years, and is more associated with a personality change rather than with parkinsonism (Wszolek et al., 2006). However, most familial mutations causing FTDP-17 have been linked to tau's role in microtubule stabilization and assembly in neurons due to their presence in the coding regions of the tau gene. Finally, in FTDP-17 autopsy samples, tau oligomers have been identified and also have been demonstrated to propagate endogenous tau pathology in the brain (Lasagna-Reeves et al., 2012); (Goedert and Spillantini, 2011); (Karch et al., 2012).

The protein-coding region of tau encodes genes involved in axonal transport, or the transport of organelles and vesicles from the soma to the synapse of neurons. Organelles such as mitochondria and lysosomes are transported *via* both anterograde and retrograde axonal transport (Chevalier-Larsen and Holzbaur, 2006; Seamster et al., 2012). In addition, the role of axonal transport has been studied in models of neurodegenerative diseases such as ALS and Alzheimer's disease (Bearer, 2012); (Seamster et al., 2012; Smith et al., 2007; Zhang et al., 2004). For example, several studies in patient cell lines (Schulz et al., 2012; Trimmer and Borland, 2005) as well as *in vivo* models of neurodegenerative diseases have demonstrated deficits in this process prior to the onset of overt pathology (Kim et al., 2011); (Chevalier-Larsen and Holzbaur, 2006; Smith et al., 2010; Trimmer and Borland, 2005). Measuring axonal transport *in vivo* is very challenging. Manganese-enhanced MRI (MEMRI) is one of the few unique methods for axonal transport assessments in a non-invasive manner (Massaad et al., 2010; Smith et al., 2010); (Silva et al., 2004). MEMRI utilizes the presence of Ca^{2+} channels in neurons in order to enter cells and be transported down their axons (Inoue et al., 2011). MEMRI has many applications and has been used to measure rates of transport in models of both hyperglycemia as well as Alzheimer's disease (Kim et al., 2009) (Fu-Hua Wang, 2012). MEMRI can also be used to measure synaptic strength *in vivo* (Serrano et al., 2008). For example, in the amyloid overproducing Tg2576 mouse model, axonal transport deficits were detected using MEMRI prior to the onset of amyloid plaque deposits in the brains of these mice, indicating that the method reliably and sensitively can detect such deficits *in vivo* and such deficits more importantly precede disease pathology (Smith et al., 2007); (Massaad et al., 2010). In addition, a study demonstrated that WT human tau in a model lacking APP was enough to significantly worsen *in vivo* axonal transport deficits (Smith et al., 2010). Other studies have also demonstrated that axonal transport rates are unaffected by tau deletion or over-expression (Perez et al., 2013; Yuan et al., 2008). Furthermore, other studies using mouse models of tauopathy have implicated *ex vivo* deficits in axonal transport at late stages in disease progression post tau pathology (Zhang et al., 2004); (Zhang et al., 2010).

In this study, we characterized axonal transport deficits in the rTg4510 transgenic line, a mouse model of FTDP-17. This well characterized model carry the human P301L mutation found in several FTDP-17 cases (Combs and Gamblin, 2012). The expression of P301L tau in the forebrain is driven by the calmodulin kinase II (CaMKII) promoter. It has also been demonstrated that the CaMKII promoter has been shown to drive expression in the olfactory bulb (Liu, 2000). The phenotype of this mouse has also been used to test biomarker serum levels for tau spinal fluid levels, as well as several potential antioxidant biomarkers (Kopeikina et al., 2011); (Berger et al., 2007). Additionally, several learning and memory assays have been used to characterize the model, and these indicate a progressive, age-related decline in both short and long term memory beginning at 4 months of age (Yue et al., 2011); (Ludvigson et al., 2011). Anatomical MRI studies have also been conducted in this mouse model at critical points in the disease process, demonstrating that neurodegeneration is isolated to the forebrain (Kopeikina et al., 2011). A recent study using the MEMRI technique has indicated a correlation between neuronal transport and tangle pathology in an alternate model (JNPL3) of tauopathy (Bertrand et al., 2013). In this study, the authors longitudinally characterized JNPL3 mice for their pathology and correlated peak values of transport rates. However, to date, a characterization of axonal transport with extensive tau isoform characterizations at each age point has not been conducted in a well-characterized FTDP-17 model such as the rTg4510 mouse model of tauopathy.

Here, we characterized axonal transport rates in the rTg4510 mouse model of tauopathy and correlated these rates to the onset of tau tangle pathology in the mouse. Our data show that axonal transport deficits precede the deposition of tau aggregates and the formation of tau fibrillary tangles that are typically associated with cognitive deficits.

2. Materials and methods

2.1. Mice and genotyping

For this study, we used mice that over-express the P301L mutation in 4R0N human tau associated with FTDP-17. The generation of rTg (tau_{P301L}) 4510 mice (abbreviated as rTg4510 mice) has been described previously (Berger et al., 2007; Ludvigson et al., 2011). These transgenic mice were generated by F1 crossing of responder mice carrying tau_{P301L} cDNA with an upstream tetracycline-operon responsive element (abbreviated as P301L) and activator mice containing a trans-activator gene consisting of the tetracycline-off open reading frame placed downstream of the CaMKII promoter (abbreviated as tTA). Both transgenic lines were gifts from Michael Hutton (Mayo Foundation) and Karen Ashe (University of Minnesota Medical School). Littermates lacking both the responder transgenes (P301L) and activator (tTA) were used as wild-type controls (NTg). For all groups, both male and female mice were used, and pilot studies were conducted prior to data collection to confirm that there were no sex differences in these measurements.

Mouse genotypes were determined from tail biopsies using real-time qPCR with specific probes designed for each gene by a commercial service (Transnetyx, Cordova, TN, USA). For accurate genotyping, tail tissues from mice were digested overnight in extraction buffer (50 mM KCl; 10 mM Tris–HCl (pH 9.0); 0.1% Triton X-100; 0.4 mg/mL Proteinase K) at 55 °C to extract genomic DNA. Human tau and CAMKII transgene were detected using the following primers: CamKII tTa forward (5′-CGC TGT GGG GCA TTT TAC TTT-3′); CamKII tTa reverse

(5′-CAT GTC CAG ATC GAA ATG GTC-3′), human tau-exon1 forward (5′-TGAACCAGGATGGCTGAGC-3′); and human tau-exon5 reverse (5′-TTGT CATCGCTTCCAGTCC-3′). PCR cycling conditions were: 94 °C (5 min), 94 °C (30 s) + 60 °C (30 s) + 72 °C (45 s) for 30 cycles, and 72 °C (10 min) using Econo Taq Plus Green Master Mix (Lucigen Corp., Middleton, WI). Animal housing and use were in compliance with the NIH Guidelines for the *Care and Use of Laboratory Animals* and were approved by the institutional animal care committee at Baylor College of Medicine. The numbers of mice used per figure are described in Supplementary Table 1.

2.2. Manganese administration

Mice were anesthetized with 5% isofluorane in 100% O_2 for 2 min in order to administer a nasal lavage of 4 μL of 0.75 g/mL $MnCl_2$ dissolved in nanopure water. Once this was administered, the animals were placed back into their cage and allowed to recover. One hour after lavage administration, the mice were exposed to 5% isoflurane and then carefully exposed to 2% isoflurane in 100% O_2 for imaging. Mice were then placed in a head holder while respiratory rate was monitored and temperature was maintained at 37 °C. This was done using an air heating system with the Model 1025 Small Animal Monitoring and Gating System Software (SA Instruments, Inc.).

2.3. MRI

All images in this study were acquired with a 9.4T, Bruker Avance Biospec Spectrometer, 21 cm bore horizontal scanner with a 35 mm volume resonator (Bruker Biospin, Billerica, MA). Imaging parameters of the olfactory MEMRI scans were: TE = 8.536 ms, TR = 504 ms, FOV = 30 mm^2, slice thickness = 1 mm, matrix = 128 × 128, NEX = 2, and number of cycles = 15 (each cycle taking about 2 min) to acquire using Paravision software (Bruker Biospin, Billerica, MA). The scan was a RARE sequence scan that was modified to have 6 slices per cycle. The first slice was consistently aligned at the most posterior point of the olfactory bulb to ensure slice reproducibility from mouse to mouse for the MEMRI scans.

2.4. MRI data analysis

All scans were analyzed using Paravision software (Bruker Biospin, Billerica, MA). The length of the olfactory bulb was measured and a line was placed on the image. From the midpoint of this line, a 90-degree angle was drawn, extending outward towards the ONL, where the region of interest (ROI) was selected. Signal intensity was measured in a ROI of one pixel in the olfactory neuronal layer (ONL) on the right side of the olfactory bulb, due to a chemical shift artifact present on the left side of the bulb (Sbarbati et al., 2002); (Smith et al., 2007). One pixel was selected due to the pixel representing one fascicle of axons that project into the olfactory neuronal layer. Single glomeruli are the target of these fascicles and one pixel minimizes outside variation from other fascicles within the olfactory epithelium (Akins and Greer, 2006). Another ROI of nine pixels was used to measure signal intensity in the water phantom. All ONL ROIs were normalized to water phantom ROIs for 15 measurements, which correspond to the 15 cycles in the scan in order to account for any differences in the shimming from mouse to mouse. This normalized signal intensity was used to plot 15 measurements per mouse. The slope of this line was then established as the axonal transport rate for each mouse. For statistical analysis, Student t tests were used to test for differences between WT and rTg4510 mice with each set of axonal transport measurements (1.5, 3, 5, and 10 month olds).

2.5. Tissue processing

Mice were sacrificed at 1.5, 3 and 6 months of age ($n = 3$ per genotype and age). The cortex was dissected and snap frozen and kept at −80 °C until use. For protein extraction, tissues were homogenized in lysis buffer consisting of 50 mM Tris (pH 7.5), 150 mM NaCl, 1 mM ethylenediaminetetraacetic acid (EDTA) (pH 8.0), 1 mM phenylmethylsulfonyl fluoride, 1% Triton X-100, protease inhibitor cocktail (Sigma, St Louis, MO, USA) and phosphatase inhibitor cocktail (Roche Applied Science, Indianapolis, IN, USA). Total protein concentration was measured using the Bradford Reagent (Thermo Scientific/Pierce Biotechnology, Rockford, IL, USA).

Ten micrograms of total protein lysate per sample was resolved by sodium dodecyl sulfate polyacrylamide gel electrophoresis and transferred onto a nitrocellulose membrane, and probed with antibodies against GFAP (1/4000; DAKO, Carpinteria, CA, USA), neurofilament medium (NF-M, 1/4000; Encore, Gainesville, FA, USA), GAPDH (1/5000; Sigma), hTAU (1/1000; DAKO), PHF-1 (1:1000, gift from Peter Davis), AT8 (1:1000, Pierce), and pSer262 tau (1:2000, Millipore). Western blot analysis was performed with infrared dye conjugated secondary antibodies, IR700 and IR800 (LI-COR Biosciences, Lincoln, NE, USA). Blots were imaged and processed on an Odyssey® Infrared Imaging System.

2.6. Immunohistochemistry

Tissue preparation and immunohistochemistry was performed as described previously (Venkitaramani et al., 2009) with slight modifications. Briefly, rTg4510 and NTg littermate mice (6-month old) were anesthetized with 5% isoflurane and transcardially perfused with ice-cold 1× phosphate buffered saline (PBS), followed by 4% paraformaldehyde (PFA) in 1× PBS. The head was removed and skinned. The brains with intact skull were post-fixed overnight in 4% PFA, extensively rinsed with 1× PBS and decalcified in 5% EDTA in 1× PBS for 2 weeks. The samples were rinsed with 1× PBS, cryopreserved in 30% sucrose in PBS and embedded in optimal cutting temperature (O.C.T.). The cryopreserved samples were sectioned along the sagittal plane at 20 μm thickness and directly mounted onto pre-cleaned/coated slides. The sections were stained as described (Venkitaramani et al., 2009) with tau antibody (HT7, 1:500, ThermoScientific/Pierce Biotechnology, Rockford, IL) and olfactory marker protein (OMP, 1:1000, Wako Chemicals, Richmond, VA). The slides were cover-slipped using ProLong Gold antifade with DAPI (Invitrogen/Molecular Probes, Eugene, OR). Immunofluorescence was visualized using Panoramic 250 scanner (3DHistech) and Nikon A1R multi-photon confocal microscope.

3. Results

In this study, we measured axonal transport rates in rTg4510 mice and age-matched littermate controls P301L-only (tau +/tta −), tTA-only (tau −/tta +), and wildtype (WT, NTg) using manganese enhanced MRI (MEMRI). Our goal was to investigate the earliest age point of microtubule-dependent transport dysfunction. We began by conducting MEMRI in 10-month old rTg4510 mice in order to verify that it was possible to use this technique without affecting mice viability. Upon observation of a reduction in Mn^{2+} transport in transgenic mice *vs.* non-transgenic mice (Fig. 1), we conducted MEMRI experiments at earlier age points. We conducted a nasal lavage of $MnCl_2$ as described in previous MEMRI work (Silva et al., 2004) and then measured the change in signal intensity over time in the olfactory neuronal layer (ONL) of the olfactory bulb using MRI. This change in signal intensity was then used to calculate a slope that is indicative of Mn^{2+} axonal transport rate.

In previous studies using rTg4510 mice, the onset of behavioral deficits and tau pathology was identified to be at 4.5 months of age (Yue et al., 2011, p. 45); (SantaCruz et al., 2005). In addition, volumetric MRI studies of both the hippocampus and cortical thickness in rTg4510 mice have indicated the onset of neurodegeneration at around 5 months (Ludvigson et al., 2011). Thus, we began measuring axonal transport rates at 5 and 10 months of age in rTg4510 mice and their

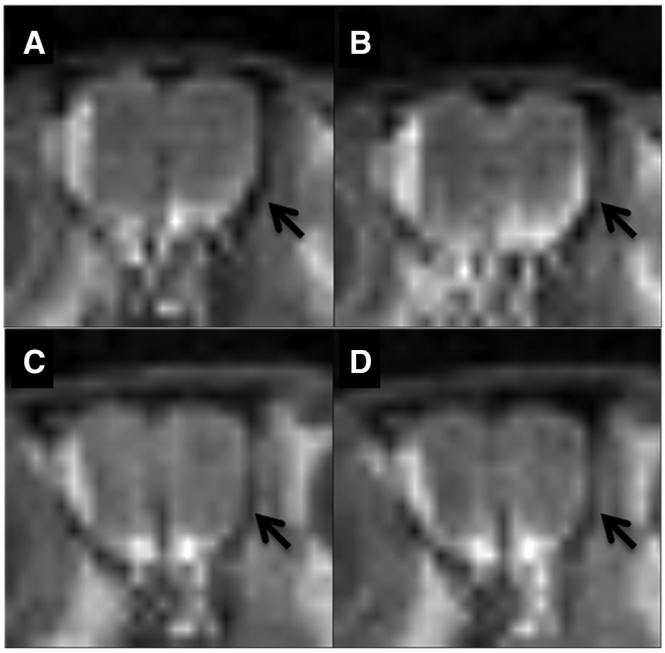

Fig. 1. Representative images from olfactory bulb slices from MEMRI scans of WT first cycle (A) and last cycle (B) and rTg4510 mice first cycle (C) and last cycle (D) 10 month old mice. The left side of the olfactory bulb contains an artifact that is present throughout all scans. Arrows on the right hand side indicate changes in signal intensity throughout multiple cycles of MEMRI scans.

littermates. We measured axonal transport of rTg4510 mice at 30% that of WT levels at 10 months of age (p-value < 0.005). At 5 months of age, we measured axonal transport rates of rTg4510 mice at 40% that of WT levels (p-value < 0.005). Thus, we observe a significant reduction in axonal transport rates in rTg4510 mice (when compared to WT/NTg mice) at both 5 and 10 months of age (Fig. 2). These results are consistent with studies examining axonal instability, the presence of tau aggregates, neurodegeneration and behavioral symptoms that have previously been characterized in this model at 5 months of age.

However, as reported previously, axonal transport deficits have preceded both the onset of behavioral deficits and amyloid pathology in other Alzheimer's disease models (Massaad et al., 2010; Smith et al., 2007). Due to this, and the large body of evidence linking the role of tau with microtubule stability in neurons (Bertrand et al., 2011; Chevalier-Larsen and Holzbaur, 2006; Smith et al., 2010; Zhang et al., 2004), we hypothesized that there could be a reduction in transport rates at an earlier time point. We observe axonal transport rates at 48% in rTg4510 mice at 3 months of age than that of WT mouse rates (p-value < 0.005) (Fig. 2). This reduction in axonal transport is a very early indicator of axonal dysfunction suggesting a significant decline in microtubule-dependent axonal transport. In order to relate these measurements to an age-dependent axonal transport dysfunction phenotype, we also evaluated the progressive change in rates in all three age groups of rTg4510 mice. Upon normalizing each measurement to the WT (NTg) control as an indicator of 100% of transport function at that age, there is approximately a 50% reduction in transport rates at 3 and 5 months, and this rate significantly reduces to 30% of the corresponding WT (NTg) mice at 10 months of age (Fig. 2).

In rTg4510 mice, the age-dependent loss of neurons and progressive cognitive dysfunction closely mimic the clinical features of tauopathy (Ishihara et al., 1999). In our model, tau with the mis-sense mutation P301L, found in some FTDP-17 cases, is over-expressed in the forebrain driven by the CaMKII promoter. From previous published data, by 2.5 months, phosphorylated tau protein and neuronal loss can be detected in the forebrain of these mice (SantaCruz et al., 2005). Cognitive impairment in spatial reference memory and synaptic dysfunction in hippocampal CA1 pyramidal neurons begin to manifest at 4.5 months of age (Hoover et al., 2010). In fact, neurodegeneration starts to become apparent after 5 months of age, primarily in the hippocampal CA1 area, becoming more prominent by 9 months of age when NFT formation and gliosis are also present in tauopathy models.

We first wanted to determine the exact time point when mutant hyperphosphorylated tau species start to appear in the cortical region of rTg4510 mice. Cortices were collected from both control and matched tau transgene overexpressing mice and probed for the common phosphorylated and pathological tau species. As is apparent from our data there is significant neurodegeneration by 6 months of age as seen from reduced neurofilament levels and increased gliosis (GFAP). However, we start observing an increased accumulation in phosphorylated tau species AT8 and pSer262 by 3 months of age (Fig. 3). The misfolded pathological tau PHF-1 was detected at 6 months of age but not in earlier age points.

Next, we wanted to verify that the mutated tau transgene was expressed in the ONL where we measured axonal transport in the rTg4510 mice. We collected olfactory bulb tissue from both transgenic and non-transgenic mice at 6 months of age. Using antibodies against total human tau (HT-7) and olfactory maker protein (OMP), we performed immunohistochemistry on these samples.

Considering that axonal transport was measured in axonal projections from olfactory sensory neurons (OSNs) to olfactory bulb (OB), we determined whether human mutant tau protein was expressed in this pathway. To establish human tau expression in OSNs as well as their processes, we performed double-labeling with human tau (Ht7) and olfactory marker protein (OMP) antibodies. We detected significant tau (green) immunostaining in the rTg4510 mice as compared to NTg controls (Fig. 4A). The axonal projections from the OSNs were co-labeled with tau and OMP (white arrowheads) in rTg4510 mice, but not in NTg controls (Fig. 4A). Within the olfactory epithelium (OE) of rTg4510 mice, we observed tau expression in OSNs that co-localized with OMP (Fig. 4B). This was absent in samples from NTg mice (Fig. 4B). These results suggest that the axonal transport deficits found in rTg4510 mice occur prior to the onset of neurofibrillary tau tangle deposition.

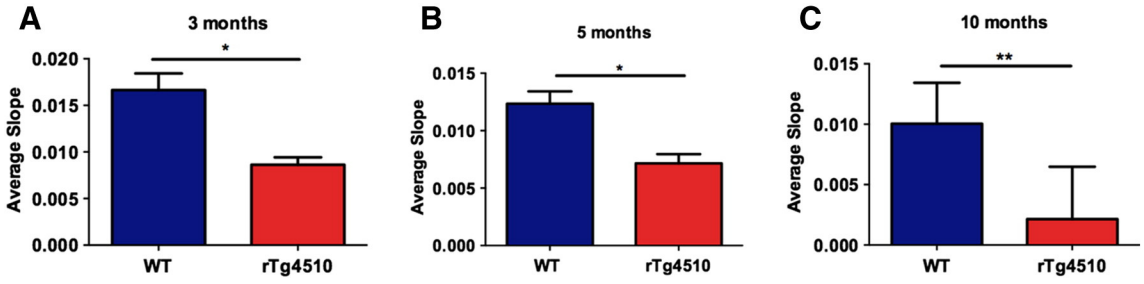

Fig. 2. Axonal transport rates in non-transgenic (WT) and rTg4510 (tau+/tta+) are displayed at 3 months with n = 6 (WT) and n = 6 (rTg4510) (A), 5 months with n = 5 (WT) and n = 5 (rTg4510) (B), and 10 months with n = 5 (WT) and n = 8 (rTg4510) (C) of age. *p < 0.05, **p < 0.005.

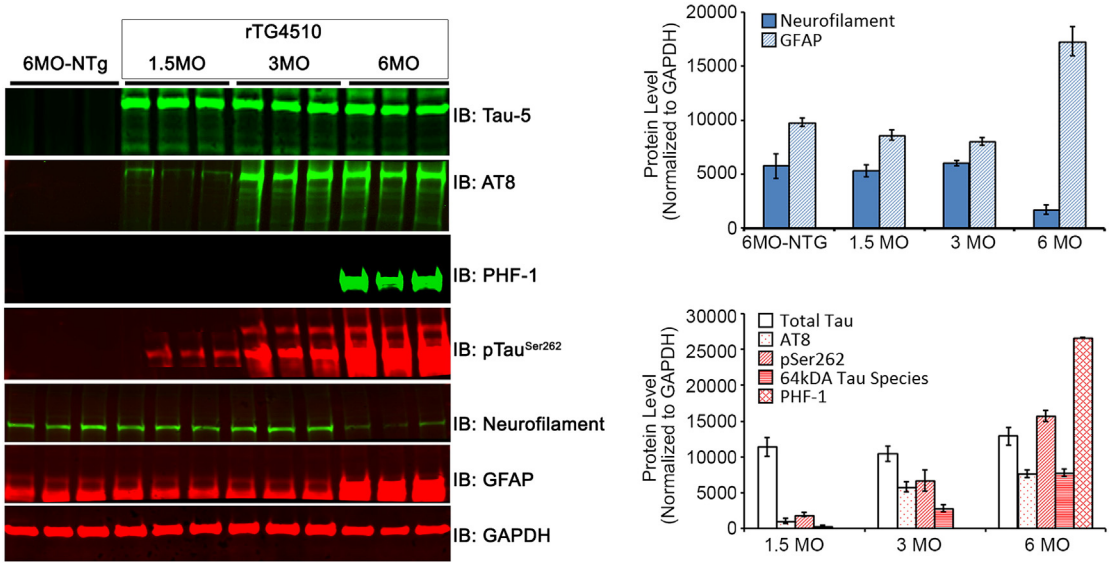

Fig. 3. Western blots show the expression of various tau species (tau 5, AT8, PHF-1, pTauSer262), neurofilament, GFAP, and GAPDH in the cortex of control and rTg4510 mice at 1, 3, and 6 months of age. N = 3 per group.

4. Discussion

It is important to identify an early biomarker of cognitive decline prior to the onset of tau tangle pathology in neurodegenerative diseases because cognitive symptoms appear several years prior to the deposits of tangles in patients (Ingram and Spillantini, 2002). In FTDP-17, familial mutations have been highly associated with onset of disease (Ingram and Spillantini, 2002; Wszolek et al., 2006). These mutations in the MAPT gene cause symptom heterogeneity of age of onset and Parkinsonian symptoms in FTDP-17 (Combs and Gamblin, 2012). However, tau tangle pathology is present in several forms of FTDP-17 and has been identified as both neurofilaments and oligomers of tau in human autopsy samples (Combs and Gamblin, 2012; Ingram and Spillantini, 2002). A large body of literature investigating tau pathology *in vitro* and *in vivo* has implicated that an earlier indicator of cognitive decline may be a destabilization of microtubules leading to a decrease in axonal transport (Bearer, 2012; Bertrand et al., 2011; Kim et al., 2011; Massaad et al., 2010; Serrano et al., 2008; Smith et al., 2010,

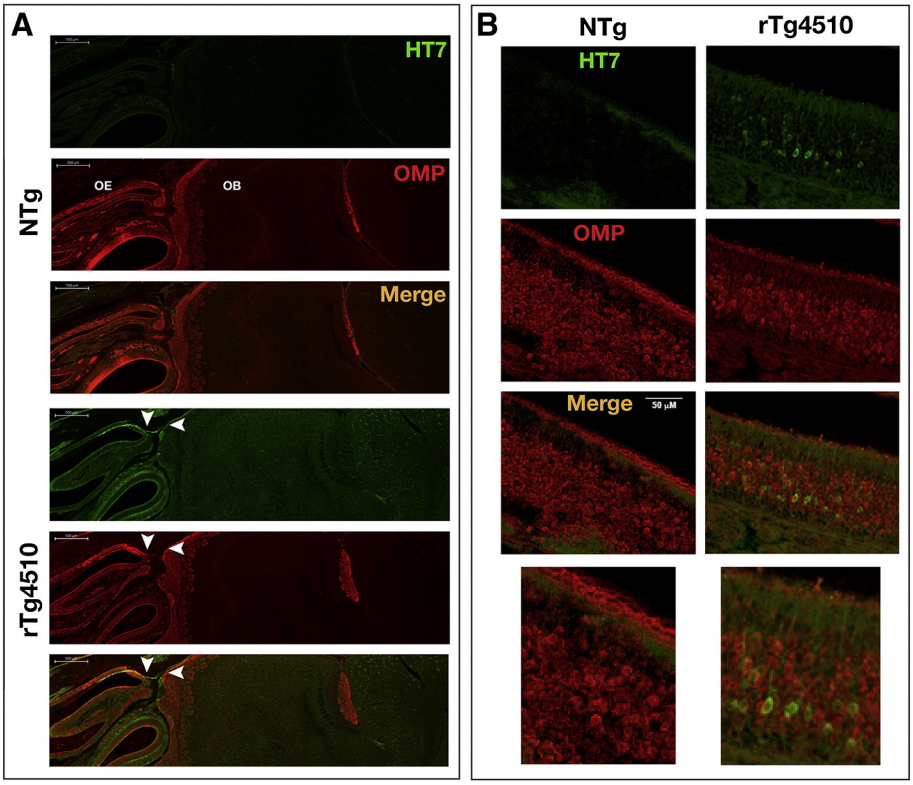

Fig. 4. Representative images of human tau (HT7) and olfactory marker protein (OMP) staining in 6-month old rTg4510 mice. (A) Sagittal brain sections from NTg and rTg4510 mice were double-labeled with antibodies that recognize human tau (HT7, green) and OMP (red). Tau expression was detected in axonal projections from olfactory sensory neurons (OSNs) to the olfactory bulb (OB) in rTg4510 mice and colocalized with OMP (white arrowheads). (B) Expression of human tau and OMP in the olfactory epithelium of NTg and rTg4510. In rTg4510 mice, tau was expressed in the cell bodies of OSNs located with the olfactory epithelium (OE).

2007). These studies not only indicate that hyperphosphorylated tau can be responsible for changes in axonal transport, but also how a decline and deregulation of ATP producing mitochondria at the synapse of neurons can cause damage to the brain (Bertrand et al., 2011).

Our study investigates this process of axonal transport using a non-invasive, *in vivo* methodology (MEMRI) in a mouse model of FTDP-17.

Axonal transport has been measured *ex vivo* in several cell culture models as well as in fixed tissue samples from both rat and mouse models of neurodegenerative diseases (Zwingmann et al., 2004) (Reddy et al., n.d.). In addition, studies have been conducted using transmission electron microscopy to measure rates of mitochondrial transport in mouse hippocampal neurons (Calkins and Reddy, 2011). However, very few studies have been able to quantify the rate of axonal transport *in vivo* in a disease environment. We and others have previously demonstrated that MEMRI can specifically measure microtubule-based transport, and it has been used in several mouse models of disease (Bertrand et al., 2013; Inoue et al., 2011; Seamster et al., 2012; Serrano et al., 2008; Smith et al., 2010, 2007; Zhang et al., 2004); (Bertrand et al., 2013; Kim et al., 2009). Additionally, MEMRI is conducted at physiologically stable temperatures and has been demonstrated to be indicative of axonal transport (Cross et al., 2008; Kim et al., 2011; Massaad et al., 2010; Millecamps and Julien, 2013; Smith et al., 2010, 2007). This study confirms and complements these previous studies and uses MEMRI to measure axonal transport for the first time in rTg4510 mice. In addition, axonal transport has been demonstrated to have an age-related decrease (Cross et al., 2008), which is then further exacerbated models with mutations found in neurodegenerative diseases. We find, similar to the models of amyloid pathology, axonal transport deficits that are present long before the onset of behavioral symptoms as well as the deposition of aggregates in the brain.

In addition, there are many forms and modifications of the tau protein that are present at various stages of disease progression in the rTg4510 mouse model of FTD. Several studies indicate that the hyperphosphorylation of tau protein is a key early indicator of dysfunction within the forebrain prior to the onset of symptoms and neurodegeneration (Hoover et al., 2010; Ishihara et al., 1999); (Hochgräfe et al., 2013). We confirm these findings by demonstrating the presence of hyperphosphorylated tau at Ser262 beginning at 3 months of age, around the same time that we begin to observe axonal transport deficits. However, the presence of PHF tau is not observed until 6 months of age in this model, which is a late stage of the disease. This indicates that the presence of some hyperphosphorylated tau species is enough to trigger the destabilization and disruption of transport in axons in FTDP-17. This can then lead to further axonal deficits as the amount increases and pathological tau species accumulate to form aggregates consisting of neurofibrillary tangles (Berger et al., 2007); (Avila et al., 2004).

In our study, we also observe the presence of human mutated tau in the olfactory bulb of rTg4510 mice. Specifically, tau in the olfactory bulb is present both in the dendritic processes and the axons of the olfactory receptor neurons. Deficits in the olfactory system are one of the earliest symptoms of some neurodegenerative diseases and recent studies have indicated that copy number variations in olfactory receptor genes are present in cohorts of patients with these diseases (Ghani et al., 2012; Shaw et al., 2011; Swaminathan et al., 2012). In parallel to the increase in severity of symptoms of patients with FTDP-17, the rTg4510 mouse model demonstrates a progressive memory impairment, neurodegeneration, as well as neurofibrillary tangle pathology (Berger et al., 2007; Kopeikina et al., 2011; Ludvigson et al., 2011; SantaCruz et al., 2005). Recent studies using microtubule stabilizing drugs have shown promising rescue of pathology in alternate tauopathy models around 5 months of age (Barten et al., 2012); (Zhang et al., 2005). However, we demonstrate that tau is altered at 3 months in the rTg4510 mouse model, in concert with the presence of both hyperphosphorylated tau species and the presence of tau oligomers at this time point and that rescue may be possible even earlier in the progression of tau aggregation and pathology.

Bertrand and colleagues have recently demonstrated a correlation between axonal transport and tau pathology in an alternate model of FTDP-17 (Bertrand et al., 2013). Their characterization of the JNPL3 model enhances the relevance of our age-related phenotype of axonal transport deficits within the olfactory bulb. They also report tau tangle pathology at 9 months of age in their model and correlate that with tau's presence as tangles within the cell bodies of neurons. Our study confirms this pathology and adds the presence of alternate phosphorylated tau species earlier in the lifespan of our mouse model as a major biochemical change at the same time point as a functional decline in axonal transport.

In addition, our study supports the extensive literature on the rTg4510 model in identifying the presence of tau tangle pathology and astrocyte involvement at 6 months of age. Finally, we are able to demonstrate a visual co-localization of the accumulation of human tau with the olfactory receptor neurons within the olfactory bulb and the axonal processes of these neurons in our mouse model. Thus, we are able to enhance and further the findings of the JNPL3 study by quantifying multiple biochemical species of tau and correlating early changes within hyperphosphorylation of human tau isoforms with the onset of age-dependent axonal transport phenotypes in the rTg4510 mouse model of FTD. Currently, clinical trials rely upon serum or cerebrospinal fluid levels of amyloid beta or tau in patients to determine efficacy of compounds. Additionally, although impairments in axonal transport have been demonstrated in human cell lines from AD patients (Stokin and Goldstein, 2006), our study adds evidence of this deficit early in the pathology of fronto-temporal dementia. Age-related declines in axonal transport (Cross et al., 2008) are exacerbated with a disease-causing mutation both in the case of amyloid beta as well as tau within the olfactory bulb. Clinically, impairments in olfaction have also been demonstrated as early indicators of the onset of neurodegeneration (Davies et al., 1993; Shaw et al., 2011). Thus, we submit that further investigations into early indicators of olfactory receptor changes and axonal transport rates in patients may provide insight into neurodegenerative disease pathology in the future.

In conclusion, we demonstrate a very early phenotype of axonal transport deficits in the rTg4510 mouse model of FTDP-17 prior to the onset of tau tangle pathology. Our study complements the growing body of evidence supporting the use of MEMRI as a reliable measurement of *in vivo* axonal transport rates and as a diagnostic indicator of cognitive decline prior to the presence of overt behavioral symptoms.

Supplementary data to this article can be found online at http://dx.doi.org/10.1016/j.nicl.2014.02.005.

Acknowledgments

The authors would like to thank Chris P. Jew, Ximin Zhou, and Taneasha W. Washington for their assistance and care of the mice during the course of this study. Funding for this work was provided by: Molecular Biology on Aging Training Grant NIH/NIA T32AG000183-20, NIH/NIA (AG029977, RGP), NIH/NINDS (NS048884, HCL), and the Belfer Neurodegeneration Consortium (MKJ, DVV, HCL, RGP).

References

Akins, M.R., Greer, C.A., 2006. Cytoskeletal organization of the developing mouse olfactory nerve layer. J. Comp. Neurol. 494, 358–367.

Avila, J., Lucas, J.J., Pérez, M., Hernández, F., 2004. Role of tau protein in both physiological and pathological conditions. Physiol. Rev. 84, 361–384.

Barten, D.M., Fanara, P., Andorfer, C., Hoque, N., Wong, P.Y.A., Husted, K.H., Cadelina, G.W., DeCarr, L.B., Yang, L., Liu, V., Fessler, C., Protassio, J., Riff, T., Turner, H., Janus, C.G., Sankaranarayanan, S., Polson, C., Meredith, J.E., Gray, G., Hanna, A., Olson, R.E., Kim, S.-H., Vite, G.D., Lee, F.Y., Albright, C.F., 2012. Hyperdynamic microtubules, cognitive deficits, and pathology are improved in tau transgenic mice with low doses of the microtubule-stabilizing agent BMS-241027. J. Neurosci. 32, 7137–7145.

Bearer, E.L., 2012. HSV, axonal transport and Alzheimer's disease: in vitro and in vivo evidence for causal relationships. Futur. Virol. 7, 885–899.

Berger, Z., Roder, H., Hanna, A., Carlson, A., Rangachari, V., Yue, M., Wszolek, Z., Ashe, K., Knight, J., Dickson, D., Andorfer, C., Rosenberry, T.L., Lewis, J., Hutton, M., Janus, C., 2007. Accumulation of pathological tau species and memory loss in a conditional model of tauopathy. J. Neurosci. 27, 3650–3662.

Bertrand, A.M., Hoang, D., Khan, U.Z., Wadghiri, Y., 2011. From axonal transport to mitochondrial trafficking: what can we learn from manganese-enhanced MRI studies in mouse models of Alzheimer's disease? Curr. Med. Imaging Rev. 7, 16–27.

Bertrand, A., Khan, U., Hoang, D.M., Novikov, D.S., Krishnamurthy, P., RajamohamedSait, H.B., Little, B.W., Sigurdsson, E.M., Wadghiri, Y.Z., 2013. Non-invasive, in vivo monitoring of neuronal transport impairment in a mouse model of tauopathy using MEMRI. NeuroImage 64, 693–702.

Bird, T.D., Nochlin, D., Poorkaj, P., Cherrier, M., Kaye, J., Payami, H., Peskind, E., Lampe, T.H., Nemens, E., Boyer, P.J., Schellenberg, G.D., 1999. A clinical pathological comparison of three families with frontotemporal dementia and identical mutations in the tau gene (P301L). Brain 122, 741–756.

Calkins, M.J., Reddy, P.H., 2011. Amyloid beta impairs mitochondrial anterograde transport and degenerates synapses in Alzheimer's disease neurons. Biochim. Biophys. Acta 1812, 507–513.

Chevalier-Larsen, E., Holzbaur, E.L.F., 2006. Axonal transport and neurodegenerative disease. Biochim. Biophys. Acta (BBA) - Mol. Basis Dis. 1762, 1094–1108.

Combs, B., Gamblin, T.C., 2012. FTDP-17 tau mutations induce distinct effects on aggregation and microtubule interactions. Biochemistry (Mosc) 51, 8597–8607.

Cross, D.J., Flexman, J.A., Anzai, Y., Maravilla, K.R., Minoshima, S., 2008. Age-related decrease in axonal transport measured by MR imaging in vivo. NeuroImage 39, 915–926.

Davies, D.C., Brooks, J.W., Lewis, D.A., 1993. Axonal loss from the olfactory tracts in Alzheimer's disease. Neurobiol. Aging 14, 353–357.

Fu-Hua Wang, P.A., Appelkvist, Paulina, Klason, Tomas, Gissberg, Olle, Bogstedt, Anna, Eliason, Kristina, Martinsson, Stefan, Briem, Sveinn, Andersson, Anders, Sandra, A., Visser, G., Ivarsson, Magnus, Lindberg, Mattias, Agerman, Karin, Sandin, Johan, 2012. Decreased axonal transport rates in the Tg2576 APP transgenic mouse: improvement with the gamma-secretase inhibitor MRK-560 as detected by manganese-enhanced MRI. European Journal of Neuroscience 36 (9), 3165–3172.

Ghani, M., Pinto, D., Lee, J.H., Grinberg, Y., Sato, C., Moreno, D., Scherer, S.W., Mayeux, R., George-Hyslop, P.S., Rogaeva, E., 2012. Genome-wide survey of large rare copy number variants in Alzheimer's disease among Caribbean Hispanics. G3 Genes Genomes Genet. 2, 71–78.

Goedert, M., Spillantini, M.G., 2011. Pathogenesis of the tauopathies. J. Mol. Neurosci. MN 45, 425–431.

Goedert, M., Ghetti, B., Spillantini, M.G., 2012. Frontotemporal dementia: implications for understanding Alzheimer disease. Cold Spring Harb. Perspect. Med. 2, a006254.

Hochgräfe, K., Sydow, A., Mandelkow, E.-M., 2013. Regulatable transgenic mouse models of Alzheimer disease: onset, reversibility and spreading of Tau pathology. FEBS J 280 (18), 4371–4381.

Hoover, B.R., Reed, M.N., Su, J., Penrod, R.D., Kotilinek, L.A., Grant, M.K., Pitstick, R., Carlson, G.A., Lanier, L.M., Yuan, L.-L., Ashe, K.H., Liao, D., 2010. Tau mislocalization to dendritic spines mediates synaptic dysfunction independently of neurodegeneration. Neuron 68, 1067–1081.

Ingram, E.M., Spillantini, M.G., 2002. Tau gene mutations: dissecting the pathogenesis of FTDP-17. Trends Mol. Med. 8, 555–562.

Inoue, T., Majid, T., Pautler, R.G., 2011. Manganese enhanced MRI (MEMRI): neurophysiological applications. Rev. Neurosci. 22, 675–694.

Ishihara, T., Hong, M., Zhang, B., Nakagawa, Y., Lee, M.K., Trojanowski, J.Q., Lee, V.M., 1999. Age-dependent emergence and progression of a tauopathy in transgenic mice overexpressing the shortest human tau isoform. Neuron 24, 751–762.

Karch, C.M., Jeng, A.T., Goate, A.M., 2012. Extracellular Tau levels are influenced by variability in Tau that is associated with tauopathies. J. Biol. Chem. 287, 42751–42762.

Kim, J., Choi, I.-Y., Michaelis, M.L., Lee, P., 2011. Quantitative in vivo measurement of early axonal transport deficits in a triple transgenic mouse model of Alzheimer's disease using manganese-enhanced MRI. NeuroImage 56, 1286–1292.

Kim,Choi, I., Michaelis, M., Lee, S., 2009. Early Impaired Axonal Transport in a Triple Transgenic Mouse Model of Alzheimer's Disease. , 17 (540).

Kopeikina, K.J., Carlson, G.A., Pitstick, R., Ludvigson, A.E., Peters, A., Luebke, J.I., Koffie, R.M., Frosch, M.P., Hyman, B.T., Spires-Jones, T.L., 2011. Tau accumulation causes mitochondrial distribution deficits in neurons in a mouse model of tauopathy and in human Alzheimer's disease brain. Am. J. Pathol. 179, 2071–2082.

Lasagna-Reeves, C.A., Castillo-Carranza, D.L., Sengupta, U., Guerrero-Munoz, M.J., Kiritoshi, T., Neugebauer, V., Jackson, G.R., Kayed, R., 2012. Alzheimer brain-derived tau oligomers propagate pathology from endogenous tau. Sci. Rep. 2.

Liu, N., 2000. Regional distribution of protein kinases in normal and odor-deprived mouse olfactory bulbs. Chem. Senses 25, 401–406.

Ludvigson, A.E., Luebke, J.I., Lewis, J., Peters, A., 2011. Structural abnormalities in the cortex of the rTg4510 mouse model of tauopathy: a light and electron microscopy study. Brain Struct. Funct. 216, 31–42.

Massaad, C.A., Amin, S.K., Hu, L., Mei, Y., Klann, E., Pautler, R.G., 2010. Mitochondrial superoxide contributes to blood flow and axonal transport deficits in the Tg2576 mouse model of Alzheimer's disease. PLoS ONE 5, e10561.

Millecamps, S., Julien, J.-P., 2013. Axonal transport deficits and neurodegenerative diseases. Nat. Rev. Neurosci. 14, 161–176.

Perez, P.D., Hall, G., Kimura, T., Ren, Y., Bailey, R.M., Lewis, J., Febo, M., Sahara, N., 2013. In vivo functional brain mapping in a conditional mouse model of human tauopathy (tau(P301L)) reveals reduced neural activity in memory formation structures. Mol. Neurodegener. 8, 9.

Reddy, P.H., Tripathi, R., Troung, Q., Tirumala, Reddy, T.P., Anekonda, V., Shirendeb, U.P., Calkins, M.J., Reddy, A.P., Mao, P., Manczak, M., n.d. Abnormal mitochondrial dynamics and synaptic degeneration as early events in Alzheimer's disease: implications to mitochondria-targeted antioxidant therapeutics. Biochim. Biophys. Acta BBA - Mol. Basis Dis.

SantaCruz, K., Lewis, J., Spires, T., Paulson, J., Kotilinek, L., Ingelsson, M., Guimaraes, A., DeTure, M., Ramsden, M., McGowan, E., Forster, C., Yue, M., Orne, J., Janus, C., Mariash, A., Kuskowski, M., Hyman, B., Hutton, M., Ashe, K.H., 2005. Tau suppression in a neurodegenerative mouse model improves memory function. Science 309, 476–481.

Sbarbati, A., Calderan, L., Nicolato, E., Marzola, P., Lunati, E., Donatella, B., Bernardi, P., Osculati, F., 2002. Magnetic resonance imaging of the rat Harderian gland. J. Anat. 201, 231–238.

Schulz, K.L., Eckert, A., Rhein, V., Mai, S., Haase, W., Reichert, A.S., Jendrach, M., Müller, W. E., Leuner, K., 2012. A new link to mitochondrial impairment in tauopathies. Mol. Neurobiol. 46, 205–216.

Seamster, P.E., Loewenberg, M., Pascal, J., Chauviere, A., Gonzales, A., Cristini, V., Bearer, E. L., 2012. Quantitative measurements and modeling of cargo-motor interactions during fast transport in the living axon. Phys. Biol. 9, 055005.

Serrano, F., Deshazer, M., Smith, K.D.B., Ananta, J.S., Wilson, L.J., Pautler, R.G., 2008. Assessing transneuronal dysfunction utilizing manganese-enhanced MRI (MEMRI). Magn. Reson. Med. 60, 169–175.

Shaw, C.A., Li, Y., Wiszniewska, J., Chasse, S., Zaidi, S.N.Y., Jin, W., Dawson, B., Wilhelmsen, K., Lupski, J.R., Belmont, J.W., Doody, R.S., Szigeti, K., 2011. Olfactory copy number association with age at onset of Alzheimer disease. Neurology 76, 1302–1309.

Silva, A.C., Lee, J.H., Aoki, I., Koretsky, A.P., 2004. Manganese-enhanced magnetic resonance imaging (MEMRI): methodological and practical considerations. NMR Biomed. 17, 532–543.

Smith, K.D.B., Kallhoff, V., Zheng, H., Pautler, R.G., 2007. In vivo axonal transport rates decrease in a mouse model of Alzheimer's disease. NeuroImage 35, 1401–1408.

Smith, K.D.B., Peethumnongsin, E., Lin, H., Zheng, H., Pautler, R.G., 2010. Increased human wildtype tau attenuates axonal transport deficits caused by loss of APP in mouse models. Magn. Reson. Insights 4, 11–18.

Snowden, J.S., Neary, D., Mann, D.M.A., 2002. Frontotemporal dementia. Br. J. Psychiatry 180, 140–143.

Stokin, G.B., Goldstein, L.S.B., 2006. Axonal transport and Alzheimer's disease. Annu. Rev. Biochem. 75, 607–627.

Swaminathan, S., Huentelman, M.J., Corneveaux, J.J., Myers, A.J., Faber, K.M., Foroud, T., Mayeux, R., Shen, L., Kim, S., Turk, M., Hardy, J., Reiman, E.M., Saykin, A.J., the Alzheimer's Disease Neuroimaging Initiative (ADNI) and the NIA-LOAD/NCRAD Family Study Group, 2012. Analysis of copy number variation in Alzheimer's disease in a cohort of clinically characterized and neuropathologically verified individuals. PLoS ONE 7, e50640.

Trimmer, P.A., Borland, M.K., 2005. Differentiated Alzheimer's disease transmitochondrial cybrid cell lines exhibit reduced organelle movement. Antioxid. Redox Signal. 7, 1101–1109.

Venkitaramani, D.V., Paul, S., Zhang, Y., Kurup, P., Ding, L., Tressler, L., Allen, M., Sacca, R., Picciotto, M.R., Lombroso, P.J., 2009. Knockout of striatal enriched protein tyrosine phosphatase in mice results in increased ERK1/2 phosphorylation. Synap. N Y C 63, 69–81.

Wszolek, Z.K., Tsuboi, Y., Ghetti, B., Pickering-Brown, S., Baba, Y., Cheshire, W.P., 2006. Frontotemporal dementia and parkinsonism linked to chromosome 17 (FTDP-17). Orphanet J. Rare Dis. 1, 30.

Yuan, A., Kumar, A., Peterhoff, C., Duff, K., Nixon, R.A., 2008. Axonal transport rates in vivo are unaffected by tau deletion or overexpression in mice. J. Neurosci. Off. J. Soc. Neurosci. 28, 1682.

Yue, M., Hanna, A., Wilson, J., Roder, H., Janus, C., 2011. Sex difference in pathology and memory decline in rTg4510 mouse model of tauopathy. Neurobiol. Aging 32, 590–603.

Zhang, B., Higuchi, M., Yoshiyama, Y., Ishihara, T., Forman, M.S., Martinez, D., Joyce, S., Trojanowski, J.Q., Lee, V.M.-Y., 2004. Retarded axonal transport of R406W mutant tau in transgenic mice with a neurodegenerative tauopathy. J. Neurosci. Off. J. Soc. Neurosci. 24, 4657–4667.

Zhang, B., Maiti, A., Shively, S., Lakhani, F., McDonald-Jones, G., Bruce, J., Lee, E.B., Xie, S.X., Joyce, S., Li, C., Toleikis, P.M., Lee, V.M.-Y., Trojanowski, J.Q., 2005. Microtubule-binding drugs offset tau sequestration by stabilizing microtubules and reversing fast axonal transport deficits in a tauopathy model. Proc. Natl. Acad. Sci. U. S. A. 102, 227–231.

Zhang, Y., Zhang, H.-M., Shi, Y., Lustgarten, M., Li, Y., Qi, W., Zhang, B.-X., Van Remmen, H., 2010. Loss of manganese superoxide dismutase leads to abnormal growth and signal transduction in mouse embryonic fibroblasts. Free Radic. Biol. Med. 49, 1255–1262.

Zwingmann, C., Leibfritz, D., Hazell, A.S., 2004. Brain energy metabolism in a sub-acute rat model of manganese neurotoxicity: an ex vivo nuclear magnetic resonance study using [1-13C]glucose. Neurotoxicology 25, 573–587.